

# A GAUSS-LAGUERRE ANALYSIS OF THE DUAL-MODE ('POTTER') HORN

Joakim F. Johansson



The Millimeter Wave Laboratory

Department of Radio & Space Science  
with Onsala Space Observatory  
Chalmers University of Technology  
S-412 96 Gothenburg  
Sweden

## ABSTRACT

The dual-mode conical horn (a.k.a. the Potter horn) has the advantage of the relative simplicity with which it can be machined, even at small dimensions. Dual-mode horns are thus often used as substitutes for corrugated horns which are lossy and difficult (or impossible) to fabricate for submillimeter wavelengths.

A dual-mode horn with the proper combination of the circular  $TE_{11}$  and  $TM_{11}$  modes has a highly symmetrical aperture field and a relatively low cross-polarization level ( $\approx 1,4$  % of the total radiated power). The fundamental Gaussian mode power fraction of the dual-mode horn ( $\approx 96,3$  %) compares well with that of the corrugated horn ( $\approx 98,1$  %).

The aperture field of the dual-mode horn has been expanded into Gauss-Laguerre modes. The symmetries of the aperture field result in a Gauss-Laguerre expansion of orders zero and two for the co-polarized part, and order two for the cross-polarized part. The expansion is rapidly convergent and truncating beyond mode number 10 would only leave out 0,026 % of the total power.

The equivalent Gaussian beam waist size and position, the radiation patterns, as well as the aperture stop requirements have been calculated and are presented as functions of the Gaussian phase slip parameter.

## 1. INTRODUCTION

At sub-millimeter wavelengths there is a never-ending quest for the Philosopher's Stone; The Optimum Antenna. An antenna should be easy to fabricate, have no loss, a very nice radiation pattern, and, of course, infinite bandwidth. But, as always, engineering is full of trade-offs. Each antenna type has its advantages and disadvantages. The corrugated conical horn [1, 2, 3] is a popular antenna for millimeter wavelengths, but they are lossy and difficult (or impossible) to fabricate for submillimeter wavelengths.

Easier to fabricate, but not that good in terms of symmetrical beams and cross-polarization properties is the smooth-walled conical horn [4].

Recently, the diagonal horn has been suggested as a candidate for shorter wavelengths. This horn yields a highly symmetrical beam, but has some cross-polarization [5, 6]. The diagonal horn is probably optimum for focal-plane imaging applications. This paper will treat the dual-mode conical horn, which combines most of the advantages of the other horns [7, 8, 9, 10]. The horn is fairly easy to fabricate, the radiation pattern is highly symmetric, the cross-polarization is low, and the smooth wall yields low losses. The main disadvantage is the rather limited bandwidth [ $\approx 5\%$ ]. In the following the dual-mode horn is described, and some definitions are made. The aperture field is then expressed in terms of Gauss-Laguerre modes, which makes it very simple to calculate the field at any point in front of the horn.

## 2. THE DUAL-MODE ('POTTER') HORN

The normal conical horn with its  $TE_{11}$  circular waveguide mode aperture field has the disadvantage of a rather non-Gaussian shape, together with abrupt field changes at the edges (E-plane). The field lines are also rather crooked, see Fig. 1. The coupling to a Gaussian beam is about 86,7 % [4], to be compared with the 98,1 % of the corrugated horn [3]. The discontinuities in the field also gives rise to marked diffractive effects, and the side-lobe level is thus fairly high in the E-plane.

The  $TE_{11}$  mode has a twin in the  $TM_{11}$  mode. The aperture field of this mode is also shown in Fig. 1. The electric field expressions for the two modes are (cf. [11]):

$$\begin{aligned} \vec{E}_{TE_{11}}(r, \varphi) = E_o \left( \left[ J_o\left(\chi \frac{r}{a}\right) + J_2\left(\chi \frac{r}{a}\right) \right] \sin \varphi \hat{r} + \left[ J_o\left(\chi \frac{r}{a}\right) - J_2\left(\chi \frac{r}{a}\right) \right] \cos \varphi \hat{\varphi} \right) = \\ E_o \left( J_2\left(\chi \frac{r}{a}\right) \sin 2\varphi \hat{x} + \left[ J_o\left(\chi \frac{r}{a}\right) - J_2\left(\chi \frac{r}{a}\right) \cos 2\varphi \right] \hat{y} \right) \end{aligned} \quad (1a)$$

$$J_1'(\chi) \equiv 0 \rightarrow \chi \approx 1,841183781$$

$$\begin{aligned} \vec{E}_{TM_{11}}(r, \varphi) = E_o \left( \left[ J_o\left(\xi \frac{r}{a}\right) - J_2\left(\xi \frac{r}{a}\right) \right] \sin \varphi \hat{r} + \left[ J_o\left(\xi \frac{r}{a}\right) + J_2\left(\xi \frac{r}{a}\right) \right] \cos \varphi \hat{\varphi} \right) = \\ E_o \left( -J_2\left(\xi \frac{r}{a}\right) \sin 2\varphi \hat{x} + \left[ J_o\left(\xi \frac{r}{a}\right) + J_2\left(\xi \frac{r}{a}\right) \cos 2\varphi \right] \hat{y} \right) \end{aligned} \quad (1b)$$

$$J_1(\xi) \equiv 0 \rightarrow \xi \approx 3,83170597$$

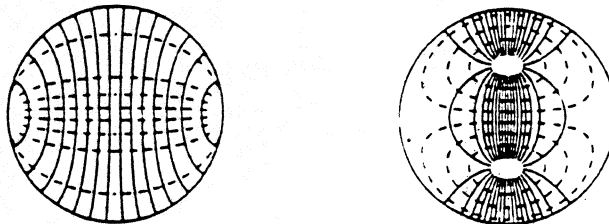


Figure 1. The electric field patterns for the circular waveguide  $TE_{11}$  (left) and  $TM_{11}$  (right) modes (cf. [11, 12]).

The two expressions are seen to have marked similarities. It is also evident that the field lines, if combined, would be straightened out. Thus the combination of these two modes can yield a much 'nicer' aperture field, given by

$$\bar{E}(r, \varphi) = \frac{\bar{E}_{TE_{11}}(r, \varphi) + \beta \bar{E}_{TM_{11}}(r, \varphi)}{1 + \beta} \quad r \leq a \quad (2)$$

where  $\beta$  is a complex mode balance constant. The total aperture field then takes the form

$$\bar{E}(r, \varphi) = E_o \left( -G\left(\frac{r}{a}\right) \sin 2\varphi \hat{x} + \left[ F\left(\frac{r}{a}\right) + G\left(\frac{r}{a}\right) \cos 2\varphi \right] \hat{y} \right) \quad (3)$$

$$F(\rho) = \frac{J_o(\chi\rho) + \beta J_o(\xi\rho)}{1 + \beta} \quad G(\rho) = \frac{-J_2(\chi\rho) + \beta J_2(\xi\rho)}{1 + \beta}$$

The idea for the dual-mode horn is thus to excite some amount of the  $TM_{11}$  mode in a mode converter and then make sure that the two modes have the correct relationship at the aperture of the conical part of the horn, see Fig. 2. Since the two modes have different cut-off frequencies, their dispersion characteristics are different. If some freedom of choice is needed in terms of horn dimensions, a phasing section is needed to ensure that the proper aperture field is achieved. All this combined makes the horn rather frequency sensitive, but this is not so important for some applications.

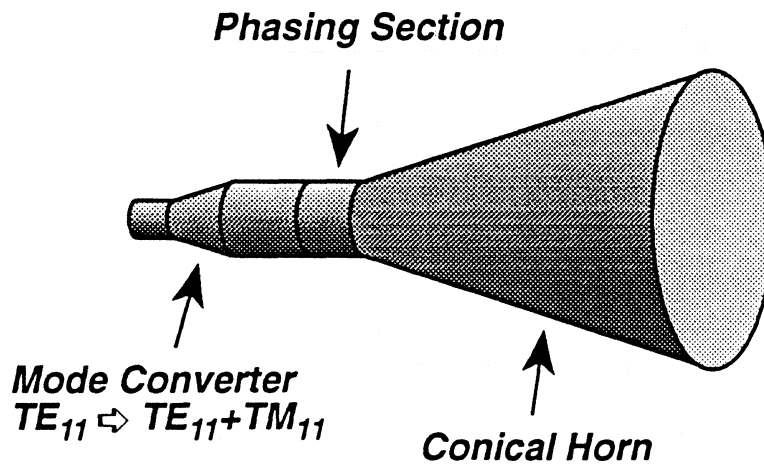


Figure 2. A schematic drawing of a dual-mode conical horn.

There are several ways to choose the relative magnitudes and phases of the two modes at the aperture plane, depending on if one wants to optimize cross-polarization, minimize sidelobes, etc. (cf. [7, 8, 13]). One way to arrange the mode excitation is to have the two modes in phase at the aperture with the mode balance constant  $\beta$

chosen so that the radial field component is zero at the rim of the horn [8], viz.

$$\beta = \frac{J_0(\chi)}{J_2(\xi)} \approx 0,7846565074 \quad (4)$$

The resulting aperture field functions are then (see Fig. 3)

$$F(\rho) = \frac{J_0(\chi) J_0(\xi \rho) - J_0(\xi) J_0(\chi \rho)}{J_0(\chi) - J_0(\xi)} \quad (5)$$

$$G(\rho) = \frac{J_2(\chi) J_2(\xi \rho) - J_2(\xi) J_2(\chi \rho)}{J_0(\chi) - J_0(\xi)}$$

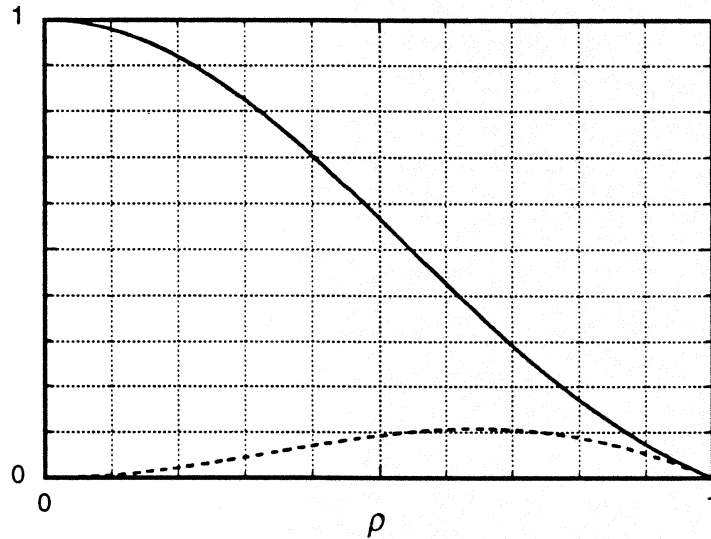


Figure 3. The functions  $F(\rho)$  (solid) and  $G(\rho)$  (dotted).

The total co-polarized field is plotted in Fig. 4. It is seen that the field is zero all along the rim of the aperture (which is seen from inspecting (5)). The aperture field is not fully circularly symmetrical, but the difference is seen to be rather small.

If one calculates the fraction of the power contained in the circularly symmetric part, as well as the co- and cross-polarized azimuthally varying parts, then the result is

$$\frac{P_{sym}^{co}}{P_{tot}} = \frac{1}{2} + \frac{\xi^2 + \chi^2}{\chi^2(\xi^2 - \chi^2)} \approx 0,9721053 \quad (6)$$

$$\frac{P_{azi}^{co}}{P_{tot}} = \frac{P_{azi}^{cr}}{P_{tot}} = \frac{1}{4} - \frac{\xi^2 + \chi^2}{2\chi^2(\xi^2 - \chi^2)} \approx 0,0139474$$

Thus, there is just a small amount 'lost' into unwanted radiation.

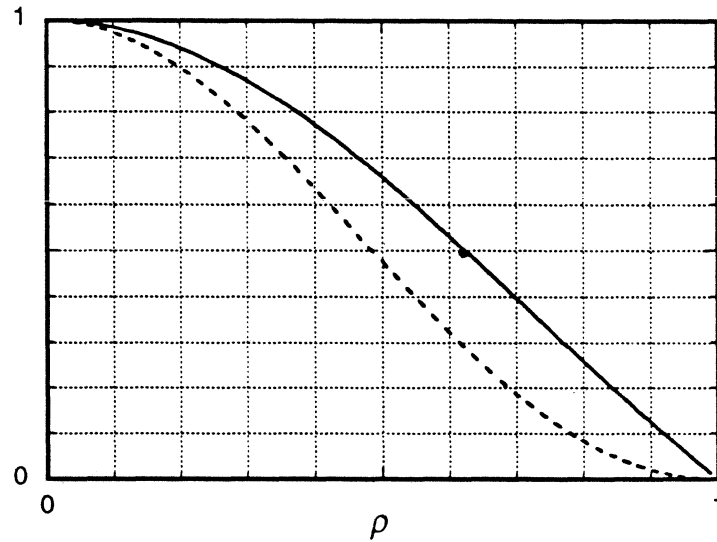


Figure 4. The co-polarized aperture field distribution plotted for two azimuthal cuts:  
 H-plane,  $\varphi = 0$  (solid)  
 E-plane,  $\varphi = \pi/2$  (dashed)

### 3. GAUSS-LAGUERRE MODES

The appearance of the aperture field in (3) gives a hint that the Gauss-Laguerre mode set would be appropriate to use in this case.

The general form for a Gauss-Laguerre expansion of a two-dimensional vector-valued function  $g$  is given by (cf. [2, 14])

$$\bar{g}(r, \varphi) = \sum_{\alpha=0}^{\infty} \sum_{n=0}^{\infty} (\bar{C}_n^{(\alpha)} \cos \alpha\varphi + \bar{S}_n^{(\alpha)} \sin \alpha\varphi) h_n^{(\alpha)}(r/w) \tag{7}$$

where the basis functions are the Gauss-Laguerre functions, viz.

$$h_n^{(\alpha)}(\rho) = \sqrt{\frac{2}{\pi}} \sqrt{\frac{2}{1 + \delta_{0\alpha}}} \sqrt{\frac{n!}{(n + \alpha)!}} (\sqrt{2}\rho)^\alpha L_n^{(\alpha)}(2\rho^2) e^{-\rho^2} \tag{8}$$

and the mode coefficients are given by

$$\begin{Bmatrix} \bar{C}_n^{(\alpha)} \\ \bar{S}_n^{(\alpha)} \end{Bmatrix} = \frac{1}{w^2} \int_0^\infty \int_0^{2\pi} \bar{g}(r, \varphi) h_n^{(\alpha)}(r/w) \begin{Bmatrix} \cos \alpha\varphi \\ \sin \alpha\varphi \end{Bmatrix} r dr d\varphi \tag{9}$$

We see that except for the zeroth-order circularly symmetric Laguerre mode set, we just have to take into account the second order sets as well. If we were to use the Gauss-Hermite expansion, a lot of these symmetry properties would be lost in a jungle of modes...

The non-zero mode coefficients of the dual-mode horn can be shown to be

$$C_{nco}^{(0)} = E_o \sqrt{2\pi} \int_0^{a^2/w^2} F\left(\frac{w}{a}\sqrt{u}\right) L_n^{(0)}(2u) e^{-u} du$$

$$C_{nco}^{(2)} = -S_{ncr}^{(2)} = \frac{E_o 2\sqrt{\pi}}{\sqrt{(n+1)(n+2)}} \int_0^{a^2/w^2} G\left(\frac{w}{a}\sqrt{u}\right) L_n^{(2)}(2u) e^{-u} u du \tag{10}$$

The choice of the parameter  $w/a$  is in principle arbitrary, but we choose to maximize the power in the fundamental mode. This criterion can be shown to be identical to finding the null for the mode coefficient  $\bar{C}_1^{(0)}$ , viz.

$$\int_0^{a^2/w^2} \left[ J_o(\xi) J_o\left(\chi \frac{w}{a} \sqrt{u}\right) - J_o(\chi) J_o\left(\xi \frac{w}{a} \sqrt{u}\right) \right] (1-2u) e^{-u} du = 0 \tag{11}$$

The result for the dual-mode aperture field is then

$$\kappa \equiv w/a = 0,5903326584$$

where a dimensionless Gaussian beam size parameter  $\kappa$  has been defined. The mode coefficients for the first few modes for this choice of parameter  $\kappa$  are given in the table below

$n$	$C_{nco}^{(0)}/E_o$	$C_{nco}^{(0)}/E_o = -S_{ncr}^{(0)}/E_o$
0	1,35876782	0,15472432
1	$\equiv 0$	0,03505191
2	-0,11945949	-0,02315560
3	-0,02464205	-0,02488684
4	0,02736328	-0,00709024
5	0,02522706	0,00698544
6	0,00468442	0,01078499
7	-0,01008692	0,00702175
8	-0,01278554	0,00083943
9	-0,00721838	-0,00388176
10	0,00041933	-0,00556457

Table I. The Gauss-Laguerre mode coefficients for a dual-mode horn when  $w/a = 0,590333$  (balanced for a null rim field).

The table shows that there are just a few dominant terms, and that the rest decay quickly with increasing mode number.

The power content in the modes is given by

$$\frac{P_n^{(\alpha)}}{P_{tot}} = w^2 \frac{\bar{C}_n^{(\alpha)} \cdot \bar{C}_n^{(\alpha)*} + \bar{S}_n^{(\alpha)} \cdot \bar{S}_n^{(\alpha)*}}{\int_0^\infty \int_0^{2\pi} \bar{g}(r, \varphi) \cdot \bar{g}(r, \varphi)^* r dr d\varphi} \tag{12}$$

Specifically, the power fraction in the fundamental mode for the dual-mode horn is

$$\frac{P_{0co}^{(0)}}{P_{tot}} = \left| \frac{w/a}{\chi} \int_0^{a^2/w^2} \left( \frac{J_0(\chi \frac{w}{a} \sqrt{u})}{J_0(\chi)} - \frac{J_0(\xi \frac{w}{a} \sqrt{u})}{J_0(\xi)} \right) e^{-u} du \right|^2 \tag{13}$$

and in our case this is

$$\kappa \equiv w/a \approx 0,5903326584 \Rightarrow \frac{P_0^{(0)}}{P_{tot}} \approx 0,9633159142$$

The number of modes that need to be included depends on the application, but a rule of thumb is that more terms are needed for near-field calculations, and for a detailed side-lobe structure. An assessment of the effects of mode set truncation can be made if one considers the fraction of the total power that is left out. If modes above  $n=10$  are excluded, then only 0,00026 of the total power is lost, and this is probably sufficient for most purposes.

The "power budget" for the dual-mode horn can be summarized as follows

Mode(s)	Power fraction
$C_{0co}^{(0)}$	0,963316
$C_{nco}^{(0)} \quad n \geq 1$	0,008789
$C_{nco}^{(2)} \quad n \geq 0$	0,013947
$S_{nco}^{(2)} \quad n \geq 0$	0,013947

Table II. The mode "power budget" for the dual-mode horn.

To get a comparison with other common submillimeter wave feed horns, the table below summarizes the properties of their respective 'Gaussicity'. It is seen that the dual-mode horn is only slightly worse than the corrugated horn in terms of coupling to the fundamental Gaussian mode. However, the corrugated horn couples to a larger waist, due to its less tapered aperture field distribution.

Horn	$\kappa = w/a$	$P_{0\text{co}}^{(0)}/P_{\text{tot}}$
Dual-Mode	0,590333	0,963316
Corrugated [3]	0,643562	0,980751
Conical [4]	0,768100	0,866621
Diagonal [5, 6]	0,863191	0,843025

Table III. A comparison between different horn antennas.

## 4. GAUSSIAN BEAM PROPAGATION

A multi-mode Gauss-Laguerre beam will propagate as [2, 3]

$$\bar{E}(r, \varphi, z) = \bar{g}(r, \varphi, [\Phi(z) - \Phi_A]) \frac{w_A}{w(z)} e^{-jk(z-z_A) + j(\Phi(z) - \Phi_A) - j \frac{kr^2}{2R(z)}} \quad (14)$$

where

$$\bar{g}(r, \varphi, \Delta\Phi) = \sum_{\alpha} \sum_n \left( \bar{C}_n^{(\alpha)} \cos \alpha\varphi + \bar{S}_n^{(\alpha)} \sin \alpha\varphi \right) h_n^{(\alpha)}(r/w) e^{-j(2n+\alpha)\Delta\Phi} \quad (15)$$

and

$$\begin{aligned} w(z) &= w_o \sqrt{1 + [z/z_c]^2} \\ R(z) &= z \left( 1 + [z_c/z]^2 \right) \\ \Phi(z) &= \arctan z/z_c \\ z_c &= \frac{\pi w_o^2}{\lambda} \end{aligned} \quad (16)$$

The beam parameters in the aperture plane of the horn are (see Fig. 5 for reference)

$$\begin{aligned} w_A &= w(z_A) = w_o \sqrt{1 + [z_A/z_c]^2} \equiv \kappa a \\ R_A &= R(z_A) = z_A \left( 1 + [z_c/z_A]^2 \right) \equiv L \\ \Phi_A &= \Phi(z_A) = \arctan z_A/z_c \end{aligned} \quad (17)$$

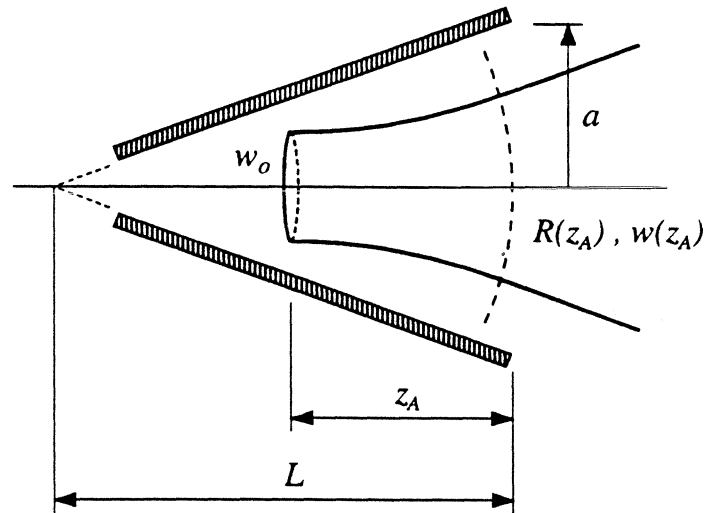


Figure 5. The geometry of a horn launching a Gaussian beam.

The equivalent waist size and position is

$$\begin{aligned}
 \Phi_A &= \arctan \frac{\pi \kappa^2 a^2}{\lambda L} \\
 w_o &= \kappa a \cos \Phi_A \\
 z_c &= \frac{L}{2} \sin 2\Phi_A \\
 z_A &= L \sin^2 \Phi_A
 \end{aligned} \tag{18}$$

It must be made clear that the equivalent waist position  $z_A$  is *not* the position of the phase center, since the different modes will combine in a complex (*sic!*) way. However, for a horn with a high fundamental Gaussian mode content, the difference between the waist position and the phase center will only be slight.

## 5. FIELD DISTRIBUTIONS AND RADIATION PATTERNS

The field distribution in a certain cut (such as the E-plane) can be found by combining (10), (14) and (15), resulting in the convenient form

$$\begin{aligned}
 E_{co}(r, \varphi, \Delta\Phi) &= E_{co}\left(r, \frac{\pi}{4}, \Delta\Phi\right) - \cos 2\varphi E_{cr}\left(r, \frac{\pi}{4}, \Delta\Phi\right) \\
 E_{cr}(r, \varphi, \Delta\Phi) &= \sin 2\varphi E_{cr}\left(r, \frac{\pi}{4}, \Delta\Phi\right)
 \end{aligned} \tag{19}$$

where the D-plane ( $\varphi = \pi/4$ ) patterns are given by

$$E_{co}\left(r, \frac{\pi}{4}, \Delta\Phi\right) = \sum_{n=0}^{\infty} C_{nco}^{(0)} h_n^{(0)}\left(\frac{r}{w}\right) e^{-j2n\Delta\Phi}$$

$$E_{cr}\left(r, \frac{\pi}{4}, \Delta\Phi\right) = \sum_{n=0}^{\infty} S_{n cr}^{(2)} h_n^{(2)}\left(\frac{r}{w}\right) e^{-j2[n+1]\Delta\Phi}$$
(20)

The different cuts are hence given by the co- and cross-polarized D-plane patterns. The field distributions when including modes  $n \leq 10$  are given in the panels in Fig. 6 as functions of the parameter  $r/w$ . If the angular far-field pattern is desired, then the following substitution should be made:

$$\frac{r}{w} \Big|_{Far-field} = \frac{\pi \kappa a}{\lambda} \cos \Phi_A \tan \theta$$

$$\Delta\Phi \Big|_{Far-field} = \frac{\pi}{2} - \Phi_A$$
(21)

where  $\theta$  is the off-boresight angle.

The -10 dB and -20 dB beamwidths calculated for the present analysis method have been checked against published data, and the results are summarized in Table IV, with the dimensions given in Table V.

Horn	E-10 dB meas.	E-10 dB calc.	E-20 dB meas.	E-20 dB calc.	H-10 dB meas.	H-10 dB calc.	H-20 dB meas.	H-20 dB calc.
Pickett et al. [9]	11,4°	13,1°	18,2°	19,2°	11,7°	11,9°	20,5°	19,7°
Ediss [10]	11,0°	11,2°	16,2°	17,4°	11,0°	11,2°	17,0°	17,9°

Table IV. The measured data from two published horns, and the corresponding calculated values for the beamwidths.

Horn	f [GHz]	a	$\gamma$ [°]	$\Phi_A$ [°]	$w_0$	$z_A$
Pickett et al.	215	3,2 $\lambda$	13,5	40,1	1,44 $\lambda$	5,53 $\lambda$
Ediss	475	4 $\lambda$	13,8	47,1	1,61 $\lambda$	8,74 $\lambda$

Table V. The data for the measured horns (from references [9 10]) and some calculated parameters.

The discrepancies are probably due to the difficulty to actually ensure that the balanced condition exists at the desired frequency, as well as differences between model and reality. In the original 'Potter' horn [7], a slightly different mode balance constant was used, and it is therefore not included in the comparison.

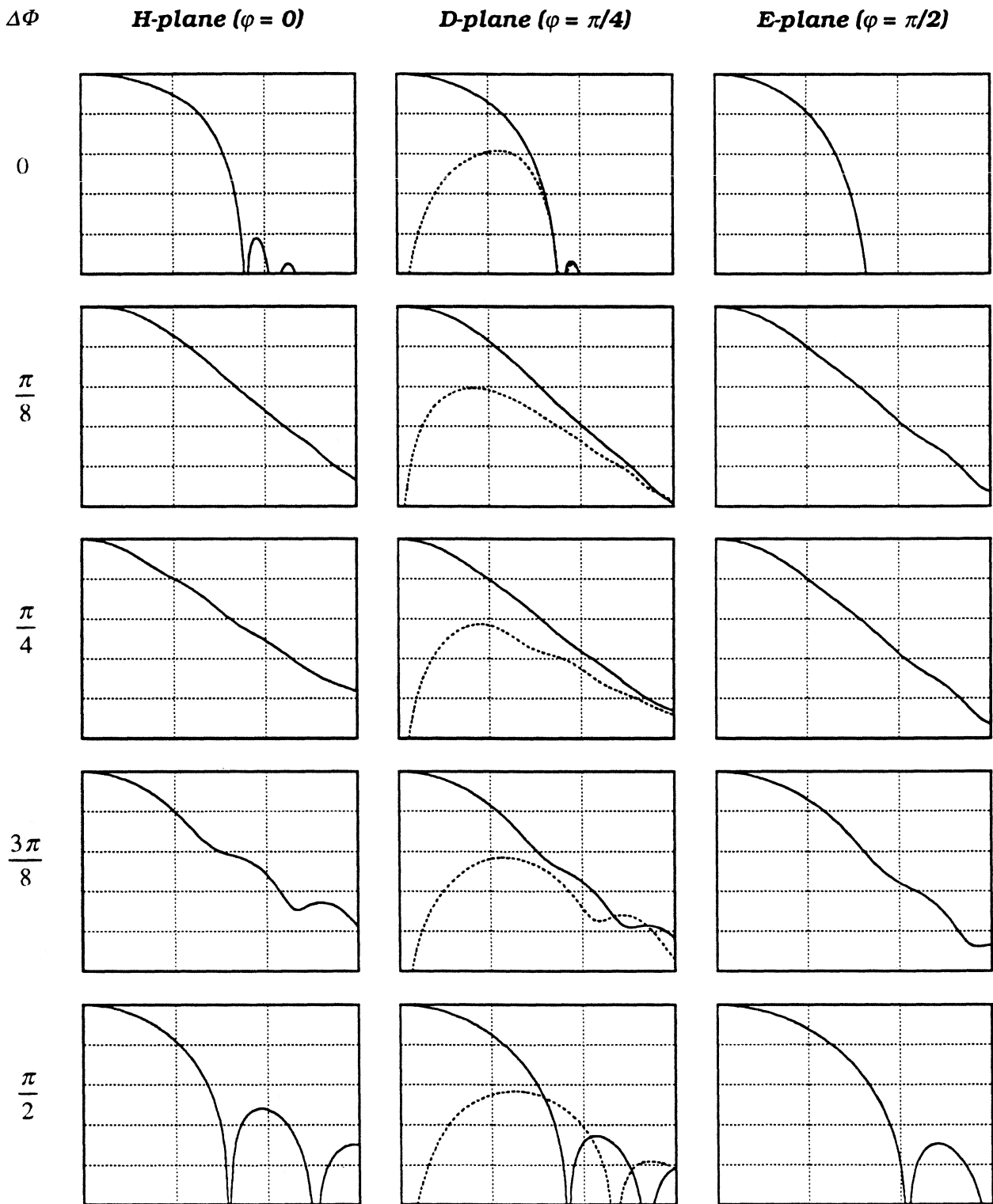


Figure 6. The field distributions for different relative phase slips  $\Delta\Phi$ . Each panel shows  $0 \leq r/w \leq 3$ , with a vertical scale from -50 dB to 0 dB. Co- (solid) and cross-pol (dotted).

## 6. VIGNETTING

An interesting property that should be studied when dealing with multi-mode Gaussian beams is where one is allowed to put an absorbing aperture stop in the path of the beam, see Fig. 7. The idealized case of just having the fundamental Gaussian mode yields that the power fraction vignetted by a circular aperture stop with a radius  $R$  is given by (cf. [1])

$$\frac{P(r \geq R)}{P_{tot}} = e^{-2R^2/w^2} \quad (22)$$

If one chooses  $R = 2w$ , then the 'lost' power fraction will be about 0,0003 . However, for a more practical, and thus finite, horn aperture distribution, the situation is more complex. The power distribution will now vary along the beam path, since the different modes combine with their respective phases.

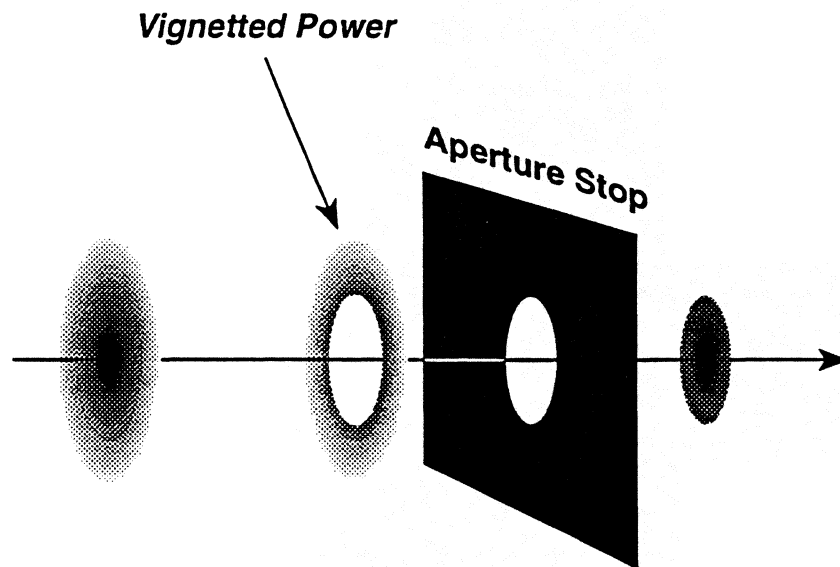


Figure 7. Vignetting of a Gaussian beam.

One can (after heavily manipulating some Laguerre polynomials) show that the power vignetted by an aperture can be written as

$$\frac{P(r \geq R)}{P_{tot}} = e^{-2R^2/w^2} \frac{\sum_{\alpha=0}^{\infty} \sum_{m=0}^{\infty} \sum_{n=0}^{\infty} Q_{mn}^{(\alpha)} \left( \frac{R}{w} \right) \left[ \bar{C}_m^{(\alpha)} \cdot \bar{C}_n^{(\alpha)*} + \bar{S}_m^{(\alpha)} \cdot \bar{S}_n^{(\alpha)*} \right] e^{-j2[m-n]\Delta\Phi}}{\sum_{\alpha=0}^{\infty} \sum_{m=0}^{\infty} \bar{C}_m^{(\alpha)} \cdot \bar{C}_m^{(\alpha)*} + \bar{S}_m^{(\alpha)} \cdot \bar{S}_m^{(\alpha)*}} \quad (23)$$

where

$$Q_{mn}^{(\alpha)}(\sigma) = \sqrt{\frac{m!n!}{(m+\alpha)!(n+\alpha)!}} e^{2\sigma^2} \int_{2\sigma^2}^{\infty} L_m^{(\alpha)}(u) L_n^{(\alpha)}(u) e^{-u} u^\alpha du \quad (24)$$

(an integral that can be expressed in a closed form!).

A contour plot for the vignetted power fraction can thus be plotted as is seen in Fig. 8. An example: a dual-mode horn with an aperture phase slip of  $\Phi_A = 45^\circ$  would thus need up to  $R = 2,7 w$  to vignette less than 0,001 of the total power in the far-field, whereas it would suffice with about  $R = 1,6 w$  close to the horn.

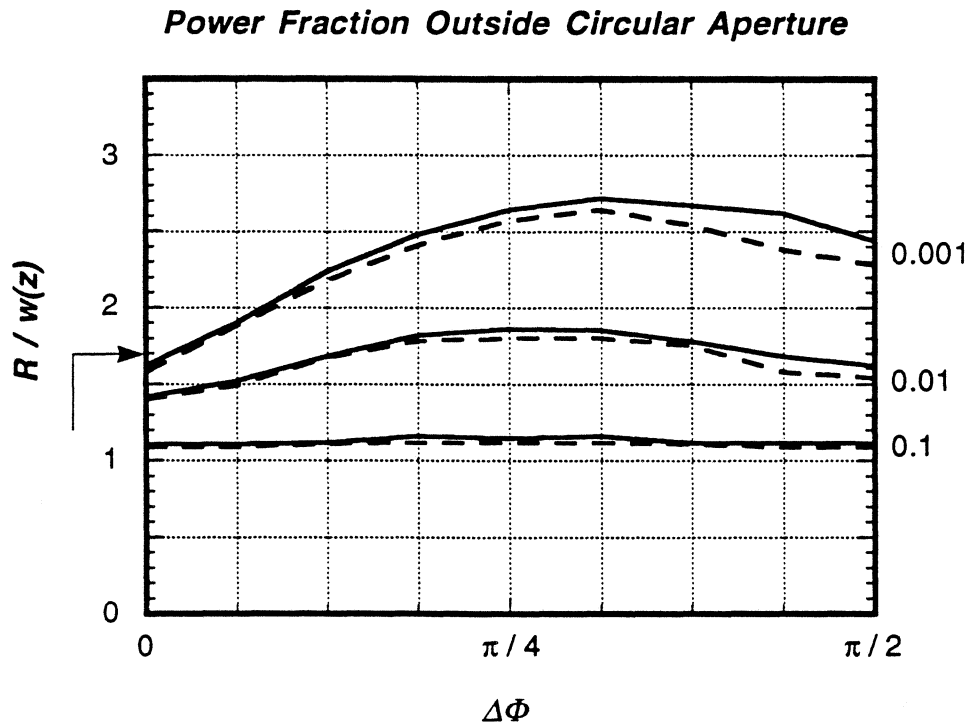


Figure 8. A contour plot for the power fraction vignetted by a circular aperture with a radius  $R$  as a function of the differential phase slip  $\Delta\Phi$  for a dual-mode horn. The arrow marks the horn aperture radius. The plot shows the cases with the cross-polarized power included (solid) and excluded (dashed).  $n \leq 10$ .

To get a 'benchmark', the corresponding plot for the corrugated conical horn is given in Fig. 9. When comparing these plots, one finds that the dual-mode horn is superior to the corrugated horn in the vignetting sense. This is due to the more tapered aperture distribution in the dual-mode horn.

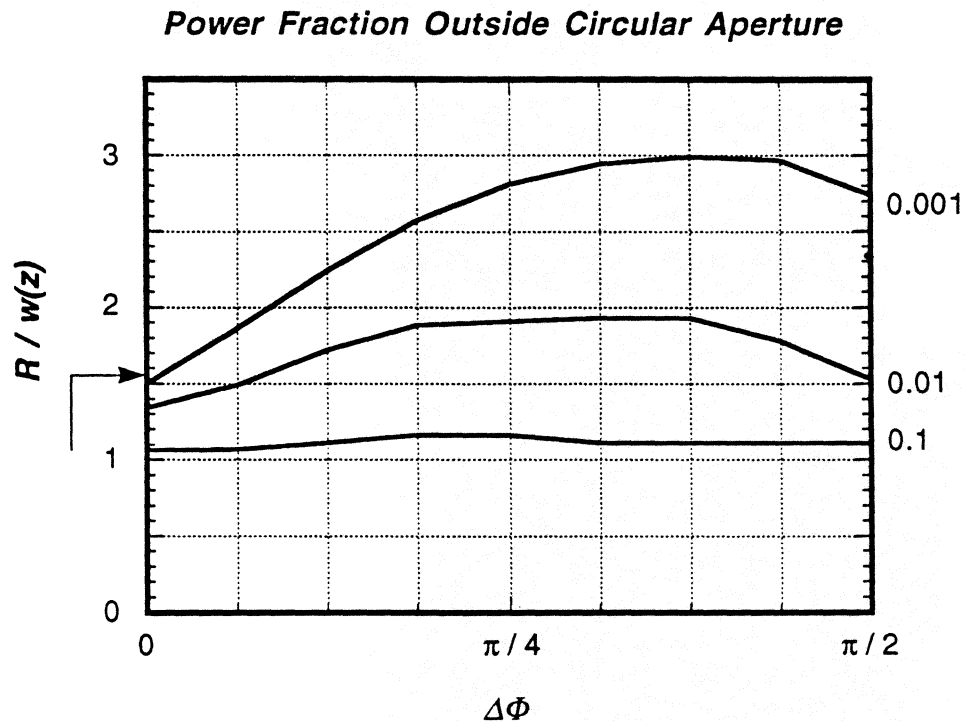


Figure 9. A contour plot for the power fraction vignetted by a circular aperture with a radius  $R$  as a function of the differential phase slip  $\Delta\Phi$  for a corrugated conical horn. The arrow marks the horn aperture radius.

## 7. CONCLUSIONS

The dual-mode conical horn has been shown to have a high coupling to the fundamental Gaussian mode. The cross-polarization and the circularly non-symmetric parts of the aperture field are very small. In some regards, such as vignetting sensitivity properties, the dual-mode horn is superior to the corrugated conical horn. The high coupling to the Gaussian beam also yields that a Gauss-Laguerre expansion only has to include just a few terms to accurately describe the field.

## ACKNOWLEDGMENTS

Financial support from the Swedish Board for Space Activities, the Swedish Council for Planning and Coordination of Research (FRN), and the Wallenberg foundation is gratefully acknowledged.

Dr. Stafford Withington, Cavendish Laboratory, Cambridge, U.K. is thanked for introducing the author to the techniques of Gaussian beam truncation calculations.

## REFERENCES

- [1] P. F. Goldsmith, "Quasi-Optical Techniques at Millimeter and Submillimeter Wavelengths", Ch. 5 in *Infrared and Millimeter Waves*, vol. 6, Ed. K.J. Button, Academic Press, 1982.
- [2] D. H. Martin *et al.*, *Millimetre-Wave Optics*, (compendium), Queen Mary College, London, U.K., 1988.
- [3] R. J. Wylde, "Millimetre-Wave Gaussian Beam-Mode Optics and Corrugated Feed Horns", IEE Proc., vol. 131, Pt. H, No. 4, pp. 258-262, Aug. 1984.
- [4] J. A. Murphy, "Aperture Efficiencies of Large Axisymmetric Reflector Antennas Fed by Conical Horns", IEEE Trans. Antennas Propagat., vol. T-AP-36, no. 4, pp. 570-575, Apr. 1988.
- [5] J. F. Johansson and N. D. Whyborn, "The Diagonal Horn as a Sub-Millimeter Wave Antenna", IEEE Trans. Microwave Theory Tech., vol. T-MTT-40, no. 5, pp. 795-800, May 1992.
- [6] S. Withington and J. A. Murphy, "Analysis of Diagonal Horns Through Gaussian-Hermite Modes", IEEE Trans. Antennas Propagat., vol. T-AP-40, no. 2, pp. 198-206, Feb. 1992.
- [7] P. D. Potter, "A New Horn Antenna with Suppressed Sidelobes and Equal Beamwidths", Microwave J., vol. VI, pp. 71-78, June 1963.
- [8] R. H. Turrin, "Dual Mode Small-Aperture Antennas", IEEE Trans. Antennas Propagat., vol. T-AP-15, pp. 307-308, March 1967.
- [9] H. M. Pickett, J. C. Hardy, and J. Farhoomand, "Characterization of a Dual-Mode Horn for Submillimeter Wavelengths", IEEE Trans. Microwave Theory Tech., vol. T-MTT-32, no. 8, pp. 936-937, Aug. 1984.
- [10] G. A. Ediss, "Dual-Mode Horns at Millimetre and Submillimetre Wavelengths", IEE Proc., vol. 132, Pt. H, No. 3, pp. 215-218, June 1985.
- [11] C. A. Balanis, *Advanced Engineering Electromagnetics*, ISBN 0-471-50316-9, Wiley, New York, 1989.
- [12] C. S. Lee, S. W. Lee, and S. L. Chuang, "Plot of Modal Field Distribution in Rectangular and Circular Waveguide", IEEE Trans. Microwave Theory Tech., vol. T-MTT-33, no. 3, pp. 271-274, March 1985.
- [13] L. Pettersson, "Dielectric Ring Mode-Generators for Dual-Mode Radiators", Research Report No. II:35, Electron Physics II, Chalmers Univ. of Technology, Gothenburg, Sweden, Jan. 1979.
- [14] A. Yariv, *Introduction to Optical Electronics*, Holt, Rinehart and Winston, Inc., New York, 1971.